ORGANOMETALLICS

pubs.acs.org/Organometallics Article

A Ru(II)−Mn(I) Supramolecular Photocatalyst for CO_2 Reduction

David C. Fabry,* Hiroki Koizumi, Debashis Ghosh, Yasuomi Yamazaki, Hiroyuki Takeda, Yusuke Tamaki, and Osamu Ishitani*

Cite This: https://dx.doi.org/10.1021/acs.organomet.9b00755 Read Online

ACCESS | Metrics & More | Article Recommendations | Supporting Information

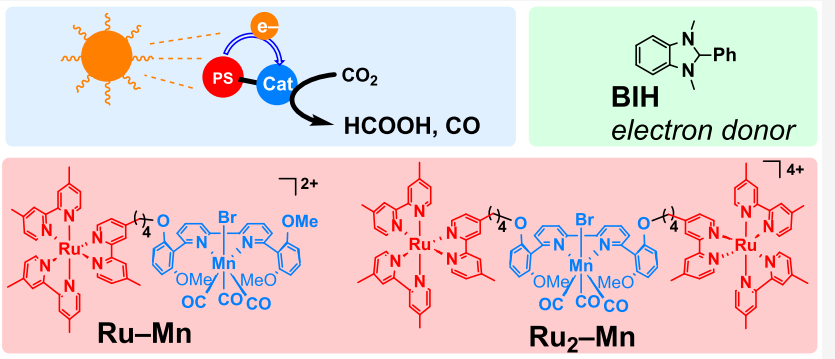

ABSTRACT: Supramolecular photocatalysts for CO_2 reduction, constituted of redox photosensitizer, catalyst, and bridging ligand, play crucial roles in constructing hybrid systems with solid materials and photoelectrochemical cells for artificial photosynthesis. We report the first supramolecular photocatalysts with a Mn(I) catalyst $[MnBr(CO)_3(BL)]$ and photosensitizer unit(s) $[Ru(dmb)_2(BL)]^{2+}$ (dmb = 4,4′-dimethyl-2,2′-bipyridine, BL = bridging ligand). A 1:1 ratio between the redox photosensitizer and catalyst units showed higher activity for HCOOH formation in comparison to the corresponding mixed system of mononuclear complexes.

INTRODUCTION

Global environment changes pose an enormous and unprecedented challenge to our society. Major contributions arise from increased emission of greenhouse gases, mainly CO_2, with more than 30 billion tons a year due to human cause.[1] Utilization of CO_2 to harvest precious chemicals or fuels by using sunlight might offer a solution for this global problem.[2] Products from CO_2 reduction are of considerable interest since they can be implemented in existing technologies: i.e., for carbon monoxide (CO) in the Fischer−Tropsch reaction.[3] Another two-electron-reduction product, formic acid (HCOOH) is a prominent candidate for hydrogen storage.[4] Molecular photocatalytic systems for CO_2 reduction require two components, i.e. a redox photosensitizer (PS) and a catalyst (CAT): the former initiates photochemical one-electron transfer from an electron donor to the CAT, and the latter accepts two electrons to reduce CO_2 to the final product(s). The CATs for selective CO_2 reduction to HCOOH are limited in comparison to the broader library for selective CO-formation catalysts.[2c] They mostly rely on Ru(II) diimine carbonyl complexes and are thereby in the range of late transition metals.[5,6] Performances of the photocatalytic systems can be greatly improved by connecting the PS and CAT with a bridging ligand, the so-called supramolecular photocatalysts.[6] For example, supramolecular photocatalysts consisting of a $[Ru(N^N)_3]^{2+}$-type PS and a $[ReCl(N^N)(CO)_3]$-type CAT (N^N = diimine ligand), connected by an alkyl chain, show much higher photocatalysis for CO_2 reduction in comparison to the mixed system of the mononuclear Ru(II) and Re(I) complexes.[7]

Recently, the catalysis of Mn(II) diimine carbonyl complexes has been extensively investigated mainly in the electrocatalytic reduction of CO_2.[8] This is because of not only the earth abundance of manganese but also the unique catalytic behavior, which is strongly dependent on the structure and electronic states of the catalyst.[9] Most of the electrocatalytic systems using Mn CATs selectively produce CO in acetonitrile-based solutions containing a proton donor. On the other hand, more recently reported photocatalytic systems consist of two-component systems with a Mn(I) CAT and $[Ru(dmb)_3]^{2+}$ (dmb = 4,4′-dimethyl-2,2′-bipyridine) or Cu(II) diimine phosphine complex as the PS. Triethanolamine (TEOA) and *N*,*N*-dimethylformamide (DMF) or *N*,*N*-dimethylacetamide (DMA) mixed solutions produced CO

Special Issue: Organometallic Chemistry for Enabling Carbon Dioxide Utilization

Received: November 5, 2019

and HCOOH with their distribution strongly dependent on the diimine ligand on the Mn CAT. *fac*-[MnBr(bpy)(CO)$_3$] (bpy = 2,2′-bipyridine), which has been frequently used as a CAT in both electrocatalytic and photocatalytic systems, tends to undergo dimerization during the catalytic CO_2 reduction due to loss of the bromide ligand from the one-electron-reduced Mn species, forming the corresponding Mn^0−Mn^0 dimer with strong visible light absorption.[9b,c]

In photocatalytic systems, the Mn^0−Mn^0 dimer photoexcitation negatively influences the photocatalysis due to its decomposition upon visible-light irradiation.[10] Incorporation of a sterically demanding diimine ligand to the Mn CAT demonstrated suppression of the dimerization,[8a,b] which would enable the application of such an Mn(I) CAT together with a PS in photochemical reactions. Although, as described above, Mn CATs have unique and fascinating properties, no supramolecular photocatalyst consisting of an Mn CAT for CO_2 reduction has ever been reported. Therefore, we herein report the first example of Ru(II)−Mn(I) supramolecular photocatalysts with bulky groups featuring the Mn CAT unit for dimer suppression, allowing selective CO_2 reduction to HCOOH (Chart 1).

Chart 1. Structures and Abbreviations of the Ru(II)−Mn(I) Supramolecular Photocatalysts and an Electron Donor for CO_2 Reduction[a]

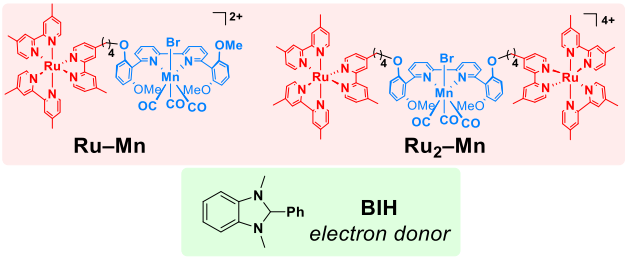

[a]The counteranion of the complexes is PF_6^-.

RESULTS AND DISCUSSION

Scheme 1 summarizes the synthesis of supramolecular photocatalysts **Ru$_x$−Mn** (x = 1, 2) and the corresponding model complex of the Mn unit (**Mn**). The synthesis of the bridging ligand was designed in a similar fashion: 2,2′-([2,2′-bipyridine]-6,6′-diyl)bis(3-methoxyphenol) (**1**) was reacted with either 1 or 2 equiv of 4-(4-bromobutyl)-4′-methyl-2,2′-bipyridine (**2**; 64% and 80% yields, respectively). For the synthesis of **BL1**, the intermediate was subsequently reacted with MeI (87% yield). The diimine ligand with bulky substituents at 6,6′-positions (6,6′-bis(2,6-dimethoxyphenyl)-2,2′-bipyridine, **MeRes**) was synthesized according to the literature.[11] The bridging ligands were respectively reacted with $RuCl_2(dmb)_2$ in EtOH/water (4/1 v/v) under microwave irradiation to give **Ru-BL** and **Ru$_2$-BL** in 48% and 64% yields. These then reacted with $MnBr(CO)_5$, giving the desired di- and trinuclear complexes (**Ru-Mn**, 84%; **Ru$_2$-Mn**, 80% yields), respectively. $MnBr(CO)_5$ reacted with **MeRes** to give **Mn** as the model for the Mn unit in a 65% yield (see Figure S6). We used [Ru(4,4-dimethyl-2,2′-bipyridine)$_3$]$^{2+}$ (**Ru**) as a model for the Ru unit.

Figure 1a shows absorption spectra of the complexes measured in DMA. The absorption spectra of **Ru-Mn** and **Ru$_2$-Mn** were generally consistent with a 1:1 and 2:1 summation of the mononuclear model complexes: i.e., **Ru** and **Mn**. This indicates that there is no strong electronic interaction between/among the subunits of the multinuclear complexes in the ground state. Broad absorptions at 400−550 and 350−500 nm are attributed to singlet metal-to-ligand charge-transfer (^{1}MLCT) transition of the Ru and Mn units, respectively.[12]

Figure 1a also shows emission spectra, which have a nearly identical broad peak shape (λ_{em} = 638 nm for **Ru-Mn** and **Ru$_2$-Mn**; λ_{em} = 636 nm for **Ru**) indicating only very weak electronic interaction between/among the excited Ru unit and the Mn unit in both **Ru-Mn** and **Ru$_2$-Mn**.

Emission quantum yields and emission decays measured in DMA indicated that intramolecular quenching of the ^{3}MLCT excited state of the Ru unit by the Mn unit did not proceed or proceeded very slowly in both **Ru-Mn** and **Ru$_2$-Mn** (Table 1 and Figure 1b). Moreover, reductive quenching rates of the emission from the Ru unit by BIH are much faster in comparison to the radiative and nonradiative decay processes; under the photocatalytic reaction conditions ([BIH] = 0.1 M), the excited Ru unit was almost quantitatively quenched by BIH, i.e. the quenching fractions (η_q) were almost 100% in **Ru**, **Ru-Mn**, and **Ru$_2$-Mn** (Figure S1). This indicates that the photocatalytic reactions in all the cases described below should be initiated by the reductive quenching of the excited Ru unit or **Ru** by BIH. The one-electron-reduced species (OERS) of **Ru** or the Ru unit are thereby generated, whereas the intramolecular electron transfer from the excited Ru unit to the Mn unit does not contribute to the photocatalytic reaction. Table 1 summarizes the photophysical data of **Ru-Mn**, **Ru$_2$-Mn**, and **Ru**.

Figure 1c shows FT-IR spectra of the complexes measured in DMA solutions under an Ar atmosphere: the spectra of **Ru-Mn** and **Ru$_2$-Mn** are clearly different from that of **Mn**. These CO-stretching bands (ν_{CO}) suggest that the equatorial coordination undergoes a slight distortion in **Ru-Mn** and **Ru$_2$-Mn** in comparison to **Mn**. This is reasonable because of increased steric hindrance and limited rotation due to connection of the much bulkier Ru unit(s) in comparison to the methyl groups.

Figure 2a shows cyclic voltammograms of the complexes measured in DMA containing Et_4NBF_4 as a supporting electrolyte under an Ar atmosphere (data are summarized in Table 2). The irreversible reduction of **Mn** was observed at E_p = −1.76 V vs Ag/$AgNO_3$. Multicycle scans change the irreversible wave to reversible one at $E_{1/2}$ = −1.58 V (Figure 2b), which is attributable to exchange of the Br^- ligand with a DMA molecule.

In the CV of **Ru-Mn**, the reduction wave of the Mn moiety was observed at slightly more negative potential (E_p = −1.79 V), which was overlapped with the first reduction of the Ru moiety. In the case of **Ru$_2$-Mn**, the reduction of the Mn moiety was shifted even more toward negative potential (E_p = −1.92 V). We can expect that, if the Ru unit electronically affects the reduction potential of the Mn moiety, the reduction wave would be shifted to a more positive potential owing to the positive charge of the Ru unit(s); actually, such phenomena were observed in both Ru-Re and Ru-Ru supramolecular photocatalysts.[6f,12a,13] In the cases of **Ru-Mn** and **Ru$_2$-Mn**, however, negative potential shifts were observed as described above. This should also indicate that the attachment of the bulky Ru unit or units at the 6,6′-position of the diimine ligand of the Mn unit caused a distorted structure of the Mn unit,

https://dx.doi.org/10.1021/acs.organomet.9b00755
Organometallics XXXX, XXX, XXX−XXX

Scheme 1. Synthesis of Ru−Mn, Ru_2−Mn, and Mn and Structure of Ru as a Model for the PS Unit[a]

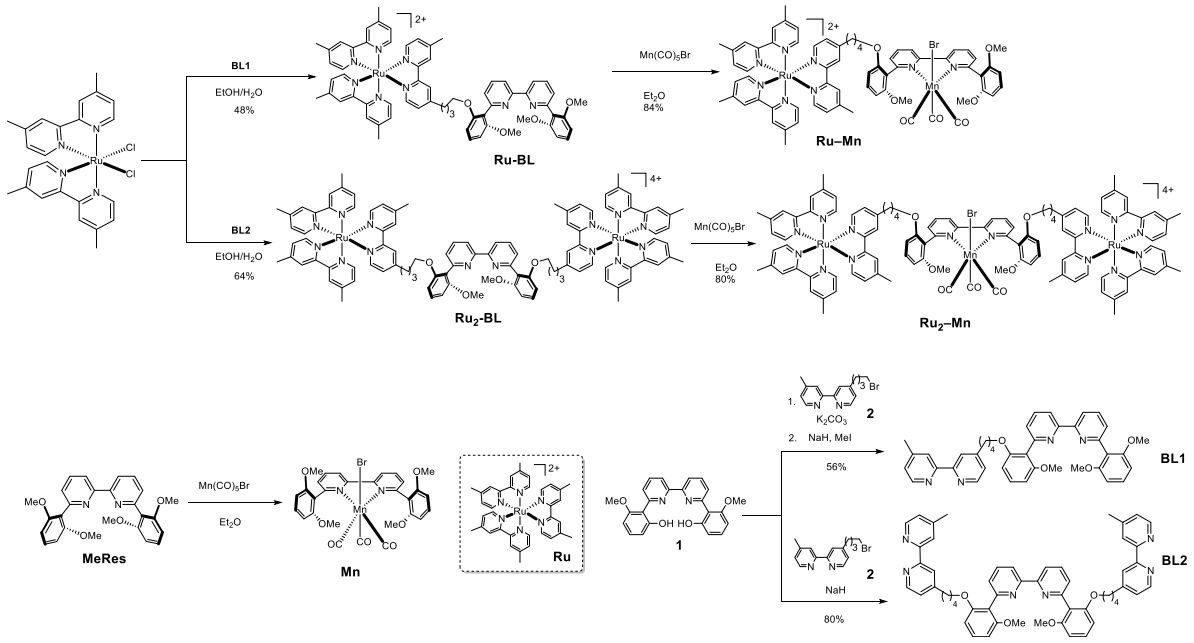

[a]The counteranion of the complexes is PF_6^-.

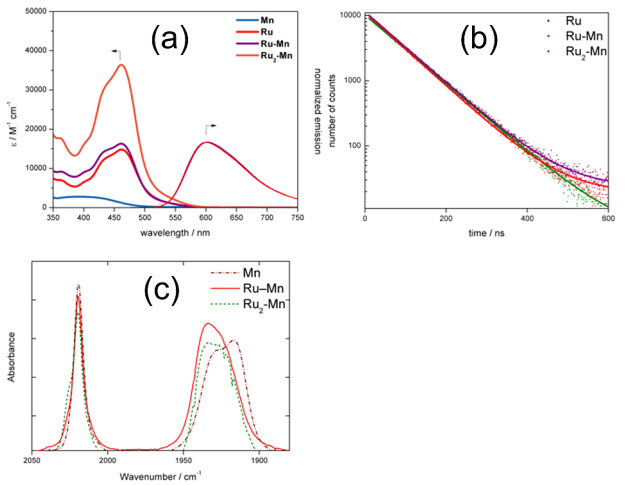

Figure 1. (a) UV−vis absorption spectra of **Ru-Mn**, **Ru_2-Mn**, **Ru**, and **Mn** complexes in DMA at 298 K and normalized emission spectra of **Ru** (purple), **Ru-Mn** (red), and **Ru_2-Mn** (green) in DMA at 298 K (λ_{ex} = 500 nm). (b) Emission decays of the **Ru** (purple), **Ru-Mn** (red), and **Ru_2-Mn** (green) in Ar-saturated DMA at 298 K (λ_{ex} = 551 nm) under deaerated conditions at 298 K. Solid lines show the fitting results. (c) FT-IR-spectra of **Mn** (purple), **Ru-Mn** (red), and **Ru_2-Mn** (green) measured in Ar-saturated DMA at 298 K.

which is the reason for the negative shift of the reduction potential of the Mn unit. Figure 2c,d shows the CVs of the complexes measured in a DMA/TEOA (4/1 v/v) mixed solution containing Et_4NBF_4 under an Ar or CO_2 atmosphere; catalytic current set off could be observed at a potential regime of $E \approx -1.8$ V in all the cases.

Photocatalytic reactions were conducted by using **Ru-Mn**, **Ru_2-Mn**, and a 1:1 mixture of **Ru** and **Mn**: the concentration of the Mn complex or the Mn unit was adjusted to be 0.05 mM. In a typical run, a 4 mL DMA/triethanolamine (4/1 v/v) solution containing **Ru-Mn** and 1,3-dimethyl-2-phenyl-2,3-dihydro-1*H*-benzo[*d*]imidazole (BIH) as an electron donor (0.1 M) was irradiated at λ_{ex} = 546 nm (light intensity 4.2 × 10^{-8} einstein s^{-1}) under a CO_2 atmosphere. We selected this irradiation wavelength because it suppressed degradation of the Mn unit owing to photochemical ligand substitution (Figure 2a).[10,12b,14]

HCOOH was produced as the main product and CO as a minor product. Only a very small amounts of H_2 were detected. Figure 3a shows time−conversion profiles of the products, and Table 3 (entry 1) summarizes the results after 6 h irradiation. The turnover numbers of the products were TON_{HCOOH} = 98 and TON_{CO} = 29, and the selectivity of the CO_2 reduction products, i.e. HCOOH + CO, was found to be $\Gamma_{HCOOH+CO}$ = 99%. In the cases using the other photocatalytic systems, similar product distributions were obtained (Table 3,

Table 1. Photophysical Properties and Quenching Behaviors of the Excited State by BIH

entry	complex	λ_{abs}[a]/nm ($\varepsilon/10^3$ M^{-1} cm^{-1})	λ_{em}[b]/nm	Φ_{em}[c]/%	τ_{em}[d]/μs	E_{00}[e]/cm^{-1}	k_q[f]/10^9 M^{-1} s^{-1}	η_q[g]/%
1	**Ru-Mn**	462 (16)	636	9.4	0.74	15960	1.1	99
2	**Ru_2-Mn**	462 (36)	636	12.4	0.79	15948	0.76	98
3	**Ru**	461 (15)	638	10.5	0.75	15901	1.1	99

[a]Maximum of the ^{1}MLCT absorption band of the Ru unit(s) or **Ru**. [b]Emission maximum measured in Ar-saturated DMA at λ_{ex} = 500 nm. [c]Quantum yield of emission measured in Ar-saturated DMA at λ_{ex} = 500 nm. [d]Emission lifetime measured in Ar-saturated DMA at λ_{ex} = 510 nm. [e]Excitation energy of the Ru unit(s) or **Ru**. [f]Quenching rate constant measured in DMA/TEOA (4/1 v/v) at λ_{ex} = 500 nm. [g]Quenching fraction of emission in the presence of 0.1 M of BIH in DMA/TEOA (4/1 v/v), which was calculated as $10k_q\tau_{em}/(1 + 0.1k_q\tau_{em})$.

https://dx.doi.org/10.1021/acs.organomet.9b00755
Organometallics XXXX, XXX, XXX−XXX

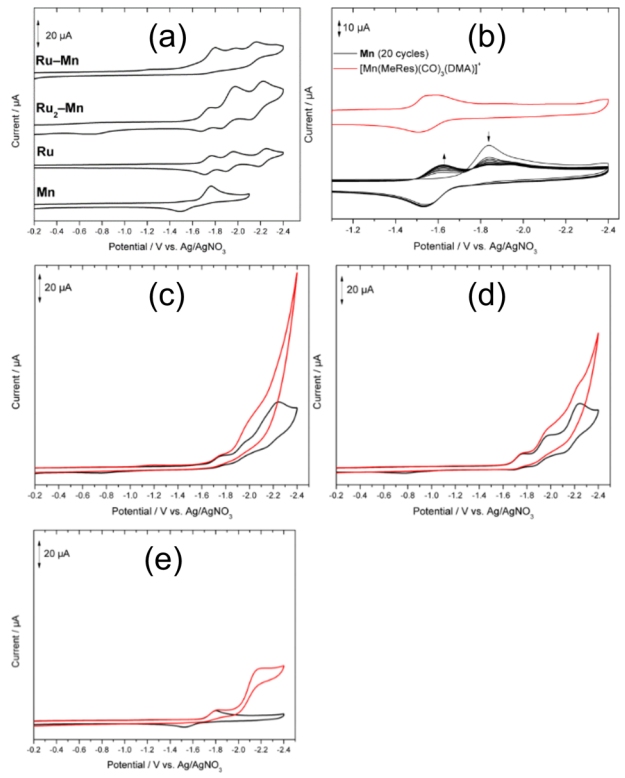

Figure 2. (a) Cyclic voltammograms of **Ru-Mn**, **Ru$_2$-Mn**, **Ru**, and **Mn** measured in DMA containing 0.1 M Et_4NBF_4 as supporting electrolyte, $Ag/AgNO_3$ (10 mM, in DMA) reference electrode, glassy-carbon-disk working electrode, Pt counter electrode, 200 mV s^{-1} scan rate. (b) Cyclic voltammograms: black, **Mn** in DMA under an Ar-atm (20 cycles); red, [Mn(**MeRes**)$(CO)_3$(MeCN)]PF_6 in DMA under an Ar atmosphere; solvent, DMA. Cyclic voltammograms: **Ru-Mn** (c), **Ru$_2$-Mn** (d), and **Mn** (e) measured in DMA/TEOA (4/1, v/v) under (black) Ar and (red) CO_2 atmospheres.

Table 2. Electrochemical Properties[a]

complex	$E_{1/2}^{Red}$/V vs Ag/Ag^+ (ΔE/mV)	$E(PS^+/PS^*)$/V[d]	$E(PS^*/PS^-)$/V[d]
Ru-Mn	−1.79,[b,c] −1.97,[c] −2.11 (124)	−1.21	0.27
Ru$_2$-Mn	−1.73 (71), −1.92 (107)[b], −2.17 (125)	−1.21	0.28
Mn	−1.76[c]		
Ru	−1.74(48), −1.93 (60), −2.22 (54)	−1.20	0.22

[a]Measured in DMA/TEOA (4/1 v/v) containing Et_4NBF_4 as a supporting electrolyte. Scan rate: 200 mV s^{-1}, [b]Overlapping waves for Mn and Ru. [c]Peak potential. [d]Excited-state oxidation and reduction potentials of the Ru unit(s) and **Ru** were calculated from $E_{1/2}^{ox} - E_{00}$ and $E_{1/2}^{red} + E_{00}$, respectively.

entries 2 and 3). However, the product formation rates strongly depended on the photocatalyst (Figure 3): using **Ru-Mn**, the formation rate of HCOOH was much faster in comparison to the mixed system of **Ru** and **Mn** and the production rate gradually slowed down after 1 h irradiation. On the other hand, the slowest rate and the lowest TON of HCOOH formation were observed in the case using **Ru$_2$-Mn**. Only in the case of the mixed system, even after 6 h irradiation, the formation rate of HCOOH did not drastically decrease. Moreover, CO was continuously produced for 6 h in all cases, with **Ru-Mn** producing the highest amount. The highest quantum yield for CO_2 reduction was obtained by using **Ru-Mn** (Φ_{HCOOH} = 14%, Φ_{CO} = 0.64%, Figure S3a,b). The mixed system of **Ru** and **Mn** showed lower yields (Φ_{HCOOH} = 11%, Φ_{CO} = 0.24%, Figure S3e,f) and efficiencies. **Ru$_2$-Mn** revealed the lowest performance (Φ_{HCOOH} = 5.4%, Φ_{CO} = 0.43%, Figure S3c,d).

The photocatalytic reactions should be initiated by reductive quenching of the Ru photosensitizer unit or **Ru** by BIH because the irradiated light (λ_{irr} = 546 nm) is absorbed by only the Ru complex but not by the Mn complex (Figure 1a) and intramolecular electron transfer from the excited Ru unit to the Mn unit does not proceed or is much slower than the reductive quenching by BIH (Table 1). The reductive quenching process quantitatively proceeded in all of the systems. However, the photocatalysis of the supramolecular photocatalyst **Ru-Mn** shows a higher performance in comparison to the mixed system consisting of **Ru** and **Mn**. At the same time, **Ru$_2$-Mn** demonstrated an even lower photocatalytic ability with respect to the mixed system. To investigate possible reasons for these differences, we measured in situ UV−vis absorption spectra of the photocatalytic reaction solutions during irradiation (Figure 4). In the case of the mixed system (**Ru** and **Mn**), no new significant absorption band was observed when the excitation light intensity was adjusted to 4.2×10^{-8} einstein s^{-1} (Figure 4c): this indicates that the photochemical reduction of **Ru** was a rate-limiting process. Actually, higher irradiation light intensity (4.8×10^{-7} einstein s^{-1}) induced both a higher CO_2 reduction rate and rapid accumulation of the one-electron-reduced species (OERS) of **Ru** (Figure S4). In the initial stage using **Ru-Mn**, only a very weak absorption change was observed until 1 h irradiation, and then a new absorption at λ_{max} = 520 nm was detected (Figure 4a). This band continuously increased over 6 h of irradiation with simultaneous depletion of absorption between 400 and 450 nm (isosbestic point at 482 nm). This spectral change is attributable to OERS accumulation of $[Ru(N^\wedge N)_3]^{2+}$ PS (N^N = diimine ligand) in solution.[12a] It should be noted that the CO formation rate slightly decreased after 1 h irradiation (Figure 3a). The fact that accumulation of the Ru-OERS in **Ru-Mn** occurred suggests that the CO_2 reduction rate of the photocatalytic system became slower than the photochemical reduction of the PS unit, probably because of decomposition of the CAT unit in **Ru-Mn**.

Figure 5 illustrates that, with increased light intensity, not only the formation of HCOOH but also accumulation of OERS in **Ru-Mn** indeed speeded up (see also Figures S4 and S5). At the same time, faster decomposition of the catalyst with increasing light intensity should proceed. The trinuclear complex **Ru$_2$-Mn** showed much faster accumulation of the OERS of the PS unit (Figure 5b); even after 30 min irradiation, the accumulated amount of OERS was larger in comparison to that after 6 h irradiation in the case using **Ru-Mn**. This strongly indicates that the electron transfer process from the OERS of the PS unit was a rate-limiting process. This is reasonable because the first reduction potential of the Mn unit in **Ru$_2$-Mn** is much more negative than that of the Ru unit as described above (Table 2), pointing toward an endergonic intramolecular electron transfer. It has been reported that excitation of the reduced $[Ru(N^\wedge N)_3]^{2+}$-type complex also induces its decomposition to give $[Ru(N^\wedge N)_2(L)_2]^{2+}$ (L = solvent), which cannot work as a redox photosensitizer.

In conclusion, we successfully synthesized a first example of supramolecular photocatalysts with the Mn(I) catalyst unit for

https://dx.doi.org/10.1021/acs.organomet.9b00755
Organometallics XXXX, XXX, XXX−XXX

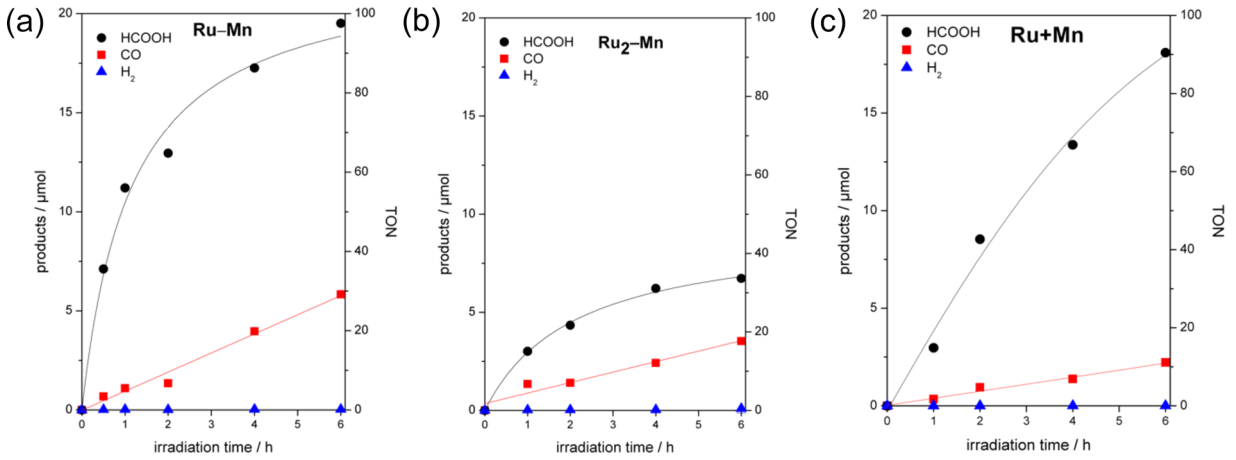

Figure 3. Irradiation−time profiles of the products in the photocatalytic reactions: a CO_2-saturated DMA/TEOA mixture (4/1 v/v, 4.0 mL) containing **Ru-Mn** (0.05 mM) and BIH (0.1 M) was irradiated at λ_{ex} = 546 nm (4.2×10^{-8} einstein s^{-1}): (a) **Ru-Mn** (0.05 mM); (b) **Ru_2-Mn** (0.05 mM); (c) [**Ru**] = [**Mn**] = 0.05 mM.

Table 3. Photocatalytic CO_2 Reduction[a]

		products/μmol (TON[b])				
entry	complex	HCOOH	CO	H_2	Γ_{HCOOH} (Γ_{CO})/%	Φ_{HCOOH} (Φ_{CO})/%
1	**Ru-Mn**	19.5 (98)	5.8 (29)	0.029 (0.1)	78 (21)	14 (0.64)
2	**Ru_2-Mn**	6.7 (33)	3.5 (18)	0.10 (0.5)	65 (34)	5.4 (0.43)
3[c]	**Ru** + **Mn**	18.1 (90)	2.2 (11)	0.006 (0.03)	89 (10)	11 (0.24)

[a]A 4.0 mL CO_2-saturated DMA/TEOA (4/1 v/v) solution containing BIH (0.1 M) and the CAT (0.05 mM) was irradiated at λ_{ex} = 546 nm (4.2×10^{-8} einstein s^{-1}) under a CO_2 atmosphere for 6 h at 298 K. [b]TON calculated by dividing the amount of the product with that of **Ru-Mn**, **Ru_2-Mn** ,or **Mn** for a mixed system. [c][**Ru**] = [**Mn**] = 0.05 mM.

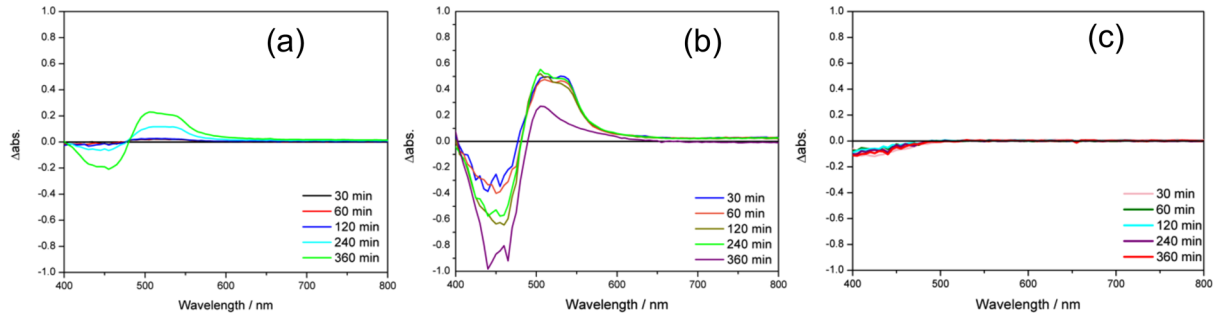

Figure 4. Differential UV−vis absorption spectra during photochemical CO_2 reduction in DMA/TEOA (4/1) at 298 K (λ_{irr} = 546 nm, 4.2×10^{-8} einstein s^{-1}) during 6 h reaction time: (a) **Ru-Mn**; (b) **Ru_2-Mn**; (c) **Ru** + **Mn**.

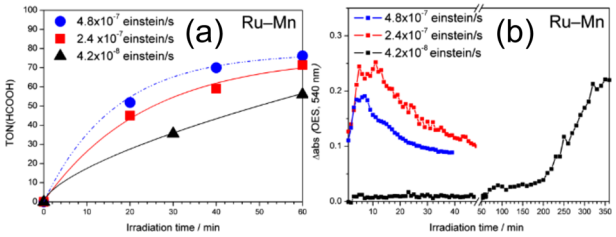

Figure 5. Effects of irradiation-light intensity on (a) HCOOH formation and (b) accumulation of the OERS of the PS unit in **Ru-Mn** during photocatalytic CO_2 reduction in DMA/TEOA (4/1) at 298 K (λ_{irr} = 546 nm).

CO_2 reduction. This Ru(II)-Mn(I) photocatalyst produced mainly HCOOH with CO as a minor product. The photocatalytic efficiency of the supramolecular photocatalyst consisting of one Ru(II) PS unit and Mn(I) CAT unit (**Ru-Mn**) was higher than that of the 1:1 mixed system of the mononuclear complexes: i.e., **Ru** and **Mn**. In contrast, photocatalysis of the trinuclear complex consisting of two Ru(II) PS units and one Mn(I) CAT unit (**Ru_2-Mn**) did not work as an efficient photocatalyst for CO_2 reduction due to slow intramolecular electron transfer from the OERS of the Ru(II) PS unit to the Mn(I) CAT unit. The distorted structure of the Mn(I) CAT unit, which is caused by the high steric hindrance of the two bulky Ru(II) PS units, induces a more negative reduction potential of the Mn CAT unit in **Ru_2-Mn** in comparison to **Mn** and **Ru-Mn**.

EXPERIMENTAL SECTION

Materials. DMA, stored over activated molecular sieves (4 Å), was freshly distilled under reduced pressure prior to use and immediately used for the reaction. TEOA was degassed under an argon atmosphere overnight prior to use and then distilled under reduced pressure. The electron donor, BIH, was synthesized according to a

https://dx.doi.org/10.1021/acs.organomet.9b00755
Organometallics XXXX, XXX, XXX−XXX

previously reported method.[6b] Tetraethylammonium tetrafluoroborate (Et_4NBF_4) for cyclic voltammetry measurements was dried in vacuo at 100 °C overnight prior to use. **Mn** was synthesized according to a previous report. All other reagents were purchased in the highest available purity and commercially obtained from Kanto Chemical Co. Inc., Wako Pure Chemical Industries, Ltd., Tokyo Chemical Industry Co., Ltd., and Sigma-Aldrich Co. LLC.

General Measurements. ^{1}H NMR spectra were recorded in a JEOL AL-400 NMR spectrometer. Electrospray ionization mass spectrometry (ESI-MS) was performed on a Shimadzu LCMS-2010A system with MeCN as the mobile phase. Electrospray ionization time-of-flight mass spectrometry (ESI-TOF-MS) was performed on a Waters LCT Premier spectrometer with MeCN as the mobile phase. UV−vis absorption spectra were recorded on a JASCO spectrometer. A Hamamatsu Photonics C-9920-02 integrating sphere with a multiphotodiode-array detector and a Horiba FluoroHub time-correlated single photon counting system were used for measuring emission quantum yields and emission lifetimes, respectively: the excitation light source was an LED pulse lamp (NanoLED, 510 nm) with an instrumental response time of less than 0.1 ns. All samples were degassed using the freeze−pump−thaw method prior to measurement. Emission quenching experiments (Figure S1) were performed in DMA/TEOA (4/1 v/v) solutions containing a complex and four different concentrations of BIH, and the quenching rate constants were calculated from slopes of the Stern−Volmer plots. An ALS/CHI Model-760Es electrochemical analyzer was used for measuring cyclic voltammograms with a glassy-carbon working electrode, a Pt counter electrode, Et_4NBF_4 as the supporting electrolyte, and $Ag/AgNO_3$ (10 mM, DMA) as the reference electrode in DMA.

Synthesis. *4-(4-(2-(6′-(2,6-Dimethoxyphenyl)[2,2′-bipyridin]-6-yl)-3-methoxyphenoxy)butyl)-4′-methyl-2,2′-bipyridine (**BL1**).* **1** (400 mg, 2.0 mmol), **2** (301 mg, 2.0 mmol), and potassium carbonate (140 mg, 2.0 mmol) were suspended in dry MeCN (20 mL) and refluxed for 16 h under an Ar atmosphere. The solvent was then removed in vacuo, the residue was redissolved in 20 mL DCM, washed with water, and dried over $MgSO_4$, and the solvent was again removed in vacuo. Recrystallization from hot acetone led to precipitation of the product, which was used in the next step without further purification. The obtained phenol (400 mg, 0.6 mmol) in 5 mL of dry THF was slowly added to a suspension of NaH (60% in mineral oil, 28 mg, 0.7 mmol, 1.1 equiv) in 10 mL of dry THF under an Ar atmosphere at room temperature. After the mixture was stirred for 5 min, MeI (60 μL, 0.96 mmol, 1.5 equiv) was slowly added and the mixture stirred for 16 h. After quenching with water, the aqueous phase was extracted with DCM (3 × 10 mL), the organic layer dried over $MgSO_4$, and the solvent removed in vacuo. Column chromatography (SiO_2, 100% DCM, 1% MeOH in DCM) yielded the desired compound **BL1** as a yellow solid. ^{1}H NMR ($CDCl_3$/δ in ppm): 8.54−8.48 (m, 2H, Ar*H*), 8.40 (t, *J* = 5.2 Hz, 1H, Ar*H*), 8.35−8.31 (m, 1H, Ar*H*), 8.25−8.04 (m, 3H, Ar*H*), 7.77−7.65 (m, 2H, Ar*H*), 7.35−7.26 (m, 3H, Ar*H*), 7.14−7.06 (m, 2H, Ar*H*), 6.89−6.83 (m, 1H, Ar*H*), 6.69−6.59 (m, 3H, Ar*H*), 3.97−3.89 (m, 3H, ArOCH_3), 3.75−3.68 (m, 8H, ArOC*H*), 2.43 (s, 3H, ArCH_3), 2.41−2.39 (m, 2H, ArCH_2), 0.90−0.80 (m, 4H, CH_2). ESI-MS: *m*/*z* 639 [M + H]. TOF-MS: calculated for $C_{40}H_{39}N_4O_4$ 639.2971, found 639.3007. As a side note, the butyl chain was chosen, because smaller linkers gave low yields during the coupling reaction or did not allow coupling at all, most likely due to steric repulsion. The butyl ether, however, gave sufficient yields.

*6,6′-Bis(2-methoxy-6-(4-(4′-methyl[2,2′-bipyridin]-4-yl)butoxy)-phenyl)-2,2′-bipyridine (**BL2**).* Following the synthesis for **BL1**, **1** (250 mg, 0.6 mmol), **2** (424 mg, 1.87 mmol, 3 equiv), and NaH (60% in mineral oil, 120 mg, 2.5 mmol, 4 equiv) were suspended in dry THF (20 mL) and stirred for 16 h under an Ar atmosphere at room temperature. The solvent was then removed in vacuo, the residue was redissolved in DCM, washed with water, and dried over $MgSO_4$, and the solvent was again removed in vacuo. Column chromatography (SiO_2, 100% DCM, 10% MeOH in DCM) yielded the desired compound **BL2** as a brown solid (423 mg, 80% yield). ^{1}H NMR ($CDCl_3$/δ in ppm): 8.61−7.58 (m, 16H, Ar*H*), 7.34−6.81 (m, 7 H, Ar*H*), 6.74−6.41 (m, 1H, Ar*H*), 3.88 (br), 3.37 (t, *J* = 6.0 Hz, 4H, OCH_2), 2.68 (t, *J* = 7.5 Hz, 4 H, ArCH_2), 2.39 (s, 6 H, ArCH_3), 1.84 (m, 8 H, CH_2). ESI-MS: *m*/*z* 871 $[M + Na]^+$ As a side note, the butyl chain was chosen, because smaller linkers gave low yields during the coupling reaction or did not allow coupling at all, most likely due to steric repulsion. The butyl ether, however, gave sufficient yields.

Ru2-BL. $RuCl_2(dmb)_2$ (203 mg, 0.4 mmol) and **BL1** (240 mg, 0.6 mmol, 1.5 equiv) were dissolved in degassed EtOH/water (4/1) in the dark and irradiated in the microwave (150 °C, 300 W) for 2 h. The solvent was then removed *in vacuo* and the residue purified via Sephadex chromatography (MeCN/water 1/1, 0−10 mM NH_4PF_6) to yield the product as a red solid (241 mg). ^{1}H NMR (MeCN-d_3/δ in ppm): 8.64−8.56 (m, 4H), 8.39−8.36 (m, 1H), 8.33 (dd, 8.1 Hz, 0.9 Hz, 1H), 8.19−8.15 (m, 1H), 7.79−7.66 (m, 1H), 7.65−7.60 (m, 2H), 7.37−7.28 (m, 10H), 7.06 (dd, 8.0, 0.8 Hz, 1H), 6.94 (dd, 7.9, 1.1 Hz, 1H), 6.77−6.69 (m, 4H), 3.97 (t, 5.0, 6 H), 3.70 (s, 3H), 3.55 (s, 6 H), 2.54−2.43 (m, 17H), 1.64−1.50 (m, 4H); ESI-MS: *m*/*z* 554 $[M - 2PF_6]$. TOF-MS: calculated for $C_{64}H_{62}F_{12}N_8O_4P_2Ru$ 554.1978, found 554.1910.

Ru-Mn. **Ru-BL** (30 mg, 21 μmol) and $MnBr(CO)_5$ (6 mg, 21 μmol) were suspended in diethyl ether in the dark under an Ar atmosphere and stirred under reflux for 16 h. After the mixture was cooled to room temperature, the product was filtered off and washed with excess diethyl ether. The product was dried in vacuo overnight and stored in the dark (29 mg, 84% yield). ^{1}H NMR (MeCN-d_3/δ in ppm): 8.53−7.95 (br, 8H, Ar*H*), 7.73−6.88 (br, 18H, Ar*H*), 6.83−6.49 (br, 4H, Ar*H*), 4.08−3.29 (br, 11H, OC*H*), 1.92 (s, 17H, ArC*H*), 1.52 (br, 4 H, C*H*); Anal. Calcd for $C_{69}H_{65}BrF_{12}MnN_9O_7P_2Ru$: C, 49.98; H, 3.95; N, 7.60. Found: C, 49.79; H, 3.87; N, 7.79. IR (DMA): 2019, 1933 cm^{-1}. As a side note, the aromatic ether groups in the supramolecular catalysts should not isomerize under the presented conditions. Known for isomerization are typically allyl phenol ethers, which are not present in the supramolecular photocatalysts.

Ru-BL. $RuCl_2(dmb)_2$ (50 mg, 0.06 mmol) and **BL2** (64 mg, 0.12 mmol, 2 equiv) were dissolved in degassed EtOH/water (4/1) in the dark and irradiated in the microwave (150 °C, 300 W) for 2 h. The solvent was then removed in vacuo and the residue purified via Sephadex chromatography (MeCN/water 1/1, 0−10 mM NH_4PF_6) to yield the product as a red solid (72 mg). ^{1}H NMR (MeCN-d_3/δ in ppm): 8.69−8.62 (m, 16H, Ar*H*), 7.85−7.77 (m, 16H, Ar*H*), 7.40−7.32 (m, 16H, Ar*H*), 3.62−3.58 (m, 6H, OCH_3), 3.39−3.33 (m, 4H, OCH_2), 2.90−2.83 (m, 4H, ArCH_2), 2.79−2.76 (m, 6H, ArCH_3), 1.86−1.80 (m, 8H, CH_2). ESI-MS: *m*/*z* 447 $[M - 4PF_6]$. Anal. Calcd for $C_{103}H_{106}Cl_2F_{30}N_{15}NaO_4P_5Ru_2$: C, 46.88; H, 4.05; N, 7.96. Found: C, 46.67; H, 3.94; N, 7.88.

Ru_2-Mn. **Ru2-BL** (50 mg, 24 μmol) and $MnBr(CO)_5$ (7 mg, 24 μmol) were suspended in diethyl ether in the dark under an Ar atmosphere and stirred under reflux for 16 h. After the mixture was cooled to room temperature, the product was filtered off and washed with excess diethyl ether. The product was dried in vacuo overnight and stored in the dark (44 mg, 80% yield). ^{1}H NMR showed diamagnetic character. Anal. Calcd for $C_{105}H_{100}BrF_{24}MnN_{14}O_7P_4Ru_2$: C, 50.93; H, 4.68; N, 7.11. Found: C, 50.92; H, 4.24; N, 7.47. IR (DMA): 2020, 1933 cm^{-1}.

Photochemical Reactions. A 4 mL DMA/TEOA mixed solution containing the photocatalyst (0.05 mM or 0.5 mM) and BIH (0.1 M) was saturated with CO_2 for 30 min. The catalyst solution was irradiated with either an Ushio Optical Module (BA-H500) high-pressure Hg lamp equipped with a 546 nm band-pass filter or a Xe short arc lamp (SX-U1500H) with a 546 nm band-pass filter. In both cases, the light intensity was adjusted by ND filters. The accurate light intensities were then determined by using $K_3Fe(C_2O_4)_3$ actinometry (4.8×10^{-7} einstein s^{-1} for the Hg lamp and 4.2×10^{-8} einstein s^{-1} for the Xe lamp), and adjusted with appropriate ND filters for the photochemical reaction. Spectral changes were monitored on a Photal MCPD-6800 photodiode array detector equipped with a MC-2530 light source. For quantum yield measurements, a Shimadzu QYM-01 quantum yield evaluation system was used in combination with an

https://dx.doi.org/10.1021/acs.organomet.9b00755
Organometallics XXXX, XXX, XXX−XXX

Asahi Spectra Co. MAX-303 300 W Xe lamp equipped with a 510 nm (fwhm 10 nm) band-pass filter. ND filters were used to adjust the light intensity. In all cases, the reaction temperature was maintained at 25 ± 0.1 °C using an IWAKI CTS-134A cooling thermos pump. The gaseous products (CO/H_2) were analyzed from the vessel head space using a GC-TCD instrument (GL science GC323) with an active carbon column. The amount of formic acid was determined by capillary electrophoresis (Otsuka Electronics Co. 7100L, pH 5.9 buffer). After photoirradiation, the solution was kept in the dark for at least 6 h to allow equilibration of the gas and liquid phase. The solution was then diluted 10 times with deionized water. A nonirradiated sample solution was analyzed as a reference, and the value was subtracted from those of the irradiated samples. In this case, the homogeneous photocatalysts cannot be separated from the solutions. For practical use of photocatalysts, it might be useful to immobilize photocatalysts on the solid surface because of easy collection of them from the reaction solution. If separation is desired, several alternative forms of such complexes have been developed that allow immobilization of the supramolecular photocatalyst on semiconductors or nonconductors. As such, they can simply be filtered off after the reaction.

■ ASSOCIATED CONTENT

Supporting Information

The Supporting Information is available free of charge at https://pubs.acs.org/doi/10.1021/acs.organomet.9b00755.

Additional figures as described in the text (PDF)

■ AUTHOR INFORMATION

Corresponding Authors

David C. Fabry − *Tokyo Institute of Technology, Tokyo, Japan*; orcid.org/0000-0003-3463-3001; Email: fabry.d.aa@m.titech.ac.jp

Osamu Ishitani − *Tokyo Institute of Technology, Tokyo, Japan*; orcid.org/0000-0001-9557-7854; Email: ishitani@chem.titech.ac.jp

Other Authors

Hiroki Koizumi − *Tokyo Institute of Technology, Tokyo, Japan*

Debashis Ghosh − *Tokyo Institute of Technology, Tokyo, Japan*

Yasuomi Yamazaki − *Tokyo Institute of Technology, Tokyo, Japan*; orcid.org/0000-0002-8640-7367

Hiroyuki Takeda − *Tokyo Institute of Technology, Tokyo, Japan*

Yusuke Tamaki − *Tokyo Institute of Technology, Tokyo, Japan*

Complete contact information is available at: https://pubs.acs.org/10.1021/acs.organomet.9b00755

Notes

The authors declare no competing financial interest.

■ ACKNOWLEDGMENTS

This work was supported by JSPS KAKENHI Grant Number JP16F16336, JSPS KAKENHI Grant Number JP17H06440 in Scientific Research on Innovative Areas "Innovations for Light-Energy Conversion (I^4LEC), and JST CREST Grant Number JPMJCR13L1 in "Molecular Technology".

■ REFERENCES

(1) Qiu, W. *Carbon Dioxide Information Analysis Center* (https://cdiac.ess-dive.lbl.gov/ (as of 1/30/2019)).

(2) (a) Nocera, D. G. Solar Fuels and Solar Chemicals Industry. *Acc. Chem. Res.* **2017**, *50*, 616−619. (b) Izumi, Y. Recent advances in the photocatalytic conversion of carbon dioxide to fuels with water and/or hydrogen using solar energy and beyond. *Coord. Chem. Rev.* **2013**, *257*, 171−186. (c) Yamazaki, Y.; Takeda, H.; Ishitani, O. Photocatalytic reduction of CO_2 using metal complexes. *J. Photochem. Photobiol., C* **2015**, *25*, 106−137. (d) Morikawa, T.; Sato, S.; Arai, T. In *Green Chemistry and Sustainable Technology: Molecular Devices for Solar Energy Conversion and Storage*; Tian, H., Boschloo, G., Hagfeldt, A., Eds.; Springer: Singapore, 2018; pp 259−280. (e) El-Khouly, M. E.; El-Mohsnawy, E.; Fukuzumi, S. Solar energy conversion: From natural to artificial photosynthesis. *J. Photochem. Photobiol., C* **2017**, *31*, 36−83.

(3) Dry, M. E. The Fischer−Tropsch process: 1950−2000. *Catal. Today* **2002**, *71*, 227−241.

(4) (a) Rice, C.; Ha, R. I.; Masel, R. I.; Waszczuk, P.; Wieckowski, A.; Barnard, T. Direct formic acid fuel cells. *J. Power Sources* **2002**, *111*, 83−89. (b) Shih, C. F.; Zhang, T.; Li, J. H.; Bai, C. L. Powering the Future with Liquid Sunshine. *Joule* **2018**, *2*, 1925−1949. (c) Li, H.; Opgenorth, P. H.; Wernick, D. G.; Rogers, S.; Wu, T. Y.; Higashide, W.; Malati, P.; Huo, Y. X.; Cho, K. M.; Liao, J. C. Integrated electromicrobial conversion of CO_2 to higher alcohols. *Science* **2012**, *335*, 1596. (d) Navarrete, A.; Centi, G.; Bogaerts, A.; Martin, A.; York, A.; Stefanidis, G. D. Harvesting Renewable Energy for Carbon Dioxide Catalysis. *Energy Techn.* **2017**, *5*, 796−811. (e) Enthaler, S. Carbon dioxide–the hydrogen-storage material of the future? *ChemSusChem* **2008**, *1*, 801−4. (f) Wang, W.-H.; Ertem, M. Z.; Xu, S.; Onishi, N.; Manaka, Y.; Suna, Y.; Kambayashi, H.; Muckerman, J. T.; Fujita, E.; Himeda, Y. Highly Robust Hydrogen Generation by Bioinspired Ir Complexes for Dehydrogenation of Formic Acid in Water: Experimental and Theoretical Mechanistic Investigations at Different pH. *ACS Catal.* **2015**, *5*, 5496−5504.

(5) (a) Ishida, H.; Terada, T.; Tanaka, K.; Tanaka, T. Photochemical carbon dioxide reduction catalyzed by bis(2,2′-bipyridine)-dicarbonylruthenium(II) using triethanolamine and 1-benzyl-1,4-dihydronicotinamide as an electron donor. *Inorg. Chem.* **1990**, *29*, 905−911. (b) Lehn, J. M.; Ziessel, R. Photochemical Reduction of Carbon-Dioxide to Formate Catalyzed by 2,2′-Bipyridine-Ruthenium-(II) or 1,10-Phenanthroline-Ruthenium(II) Complexes. *J. Organomet. Chem.* **1990**, *382*, 157−173. (c) Kuramochi, Y.; Itabashi, J.; Fukaya, K.; Enomoto, A.; Yoshida, M.; Ishida, H. Unexpected effect of catalyst concentration on photochemical CO_2 reduction by trans(Cl)-$Ru(bpy)(CO)_2Cl_2$: new mechanistic insight into the CO/HCOO(−) selectivity. *Chem. Sci.* **2015**, *6*, 3063−3074. (d) Yoshitomi, F.; Sekizawa, K.; Maeda, K.; Ishitani, O. Selective Formic Acid Production via CO_2 Reduction with Visible Light Using a Hybrid of a Perovskite Tantalum Oxynitride and a Binuclear Ruthenium(II) Complex. *ACS Appl. Mater. Interfaces* **2015**, *7*, 13092−7. (e) Kuriki, R.; Matsunaga, H.; Nakashima, T.; Wada, K.; Yamakata, A.; Ishitani, O.; Maeda, K. Nature-Inspired, Highly Durable CO_2 Reduction System Consisting of a Binuclear Ruthenium(II) Complex and an Organic Semiconductor Using Visible Light. *J. Am. Chem. Soc.* **2016**, *138*, 5159−70. (f) Kuramochi, Y.; Ishitani, O.; Ishida, H. Reaction mechanisms of catalytic photochemical CO_2 reduction using Re(I) and Ru(II) complexes. *Coord. Chem. Rev.* **2018**, *373*, 333−356.

(6) (a) In the solar fuels and photochemistry community, the term "supramolecular photocatalyst" has been established for quite some time to describe molecular photocatalysts with more than two functions, such as photosensitizer and CO_2 catalyst, in one molecule even if these units are connected by only covalent and/or coordinate bonds. For references on supramolecular catalysts, see the following. (b) Tamaki, Y.; Morimoto, T.; Koike, K.; Ishitani, O. Photocatalytic CO_2 reduction with high turnover frequency and selectivity of formic acid formation using Ru(II) multinuclear complexes. *Proc. Natl. Acad. Sci. U. S. A.* **2012**, *109*, 15673−8. (c) Tamaki, Y.; Koike, K.; Ishitani, O. Highly efficient, selective, and durable photocatalytic system for

CO_2 reduction to formic acid. *Chem. Sci.* **2015**, *6*, 7213−7221. (d) Tamaki, Y.; Ishitani, O. Supramolecular Photocatalysts for the Reduction of CO_2. *ACS Catal.* **2017**, *7*, 3394−3409. (e) Tamaki, Y.; Ishitani, O. Supramolecular photocatalysts constructed with a photosensitizer unit with two tridentate ligands for CO_2 reduction. *Faraday Discuss.* **2017**, *198*, 319−335.

(7) (a) Gholamkhass, B.; Mametsuka, H.; Koike, K.; Tanabe, T.; Furue, M.; Ishitani, O. Architecture of supramolecular metal complexes for photocatalytic CO_2 reduction: ruthenium-rhenium bi- and tetranuclear complexes. *Inorg. Chem.* **2005**, *44*, 2326−36. (b) Sato, S.; Koike, K.; Inoue, H.; Ishitani, O. Highly efficient supramolecular photocatalysts for CO_2 reduction using visible light. *Photochem. Photobio. Sci.* **2007**, *6*, 454−461. (c) Koike, K.; Naito, S.; Sato, S.; Tamaki, Y.; Ishitani, O. Architecture of supramolecular metal complexes for photocatalytic CO_2 reduction III: Effects of length of alkyl chain connecting photosensitizer to catalyst. *J. Photochem. Photobiol., A* **2009**, *207*, 109−114. (d) Kato, E.; Takeda, H.; Koike, K.; Ohkubo, K.; Ishitani, O. Ru(II)-Re(I) binuclear photocatalysts connected by -CH_2XCH_2- (X = O, S, CH_2) for CO_2 reduction. *Chem. Sci.* **2015**, *6*, 3003−3012.

(8) (a) Sampson, M. D.; Nguyen, A. D.; Grice, K. A.; Moore, C. E.; Rheingold, A. L.; Kubiak, C. P. Manganese Catalysts with Bulky Bipyridine Ligands for the Electrocatalytic Reduction of Carbon Dioxide: Eliminating Dimerization and Altering Catalysis. *J. Am. Chem. Soc.* **2014**, *136*, 5460−5471. (b) Sampson, M. D.; Kubiak, C. P. Manganese Electrocatalysts with Bulky Bipyridine Ligands: Utilizing Lewis Acids To Promote Carbon Dioxide Reduction at Low Overpotentials. *J. Am. Chem. Soc.* **2016**, *138*, 1386−1393. (c) Compain, J. D.; Bourrez, M.; Haukka, M.; Deronzier, A.; Chardon-Noblat, S. Manganese carbonyl terpyridyl complexes: their synthesis, characterization and potential application as CO-release molecules. *Chem. Commun.* **2014**, *50*, 2539−2542. (d) Bourrez, M.; Orio, M.; Molton, F.; Vezin, H.; Duboc, C.; Deronzier, A.; Chardon-Noblat, S. Pulsed-EPR Evidence of a Manganese(II) Hydroxycarbonyl Intermediate in the Electrocatalytic Reduction of Carbon Dioxide by a Manganese Bipyridyl Derivative. *Angew. Chem., Int. Ed.* **2014**, *53*, 240−243. (e) Bourrez, M.; Molton, F.; Chardon-Noblat, S.; Deronzier, A. [Mn(bipyridyl)$(CO)_3$Br]: An Abundant Metal Carbonyl Complex as Efficient Electrocatalyst for CO_2 Reduction. *Angew. Chem., Int. Ed.* **2011**, *50*, 9903−9906.

(9) (a) Tignor, S. E.; Kuo, H. Y.; Lee, T. S.; Scholes, G. D.; Bocarsly, A. B. Manganese-Based Catalysts with Varying Ligand Substituents for the Electrochemical Reduction of CO_2 to CO. *Organometallics* **2019**, *38*, 1292−1299. (b) Takeda, H.; Kamiyama, H.; Okamoto, K.; Irimajiri, M.; Mizutani, T.; Koike, K.; Sekine, A.; Ishitani, O. Highly Efficient and Robust Photocatalytic Systems for CO_2 Reduction Consisting of a Cu(I) Photosensitizer and Mn(I) Catalysts. *J. Am. Chem. Soc.* **2018**, *140*, 17241−17254. (c) Cheung, P. L.; Machan, C. W.; Malkhasian, A. Y.; Agarwal, J.; Kubiak, C. P. Photocatalytic Reduction of Carbon Dioxide to CO and HCO_2H Using *fac*-Mn(CN)(bpy)$(CO)_3$. *Inorg. Chem.* **2016**, *55*, 3192−8. (d) Francke, R.; Schille, B.; Roemelt, M. Homogeneously Catalyzed Electroreduction of Carbon Dioxide-Methods, Mechanisms, and Catalysts. *Chem. Rev.* **2018**, *118*, 4631−4701. (e) Grills, D. C.; Ertem, M. Z.; McKinnon, M.; Ngo, K. T.; Rochford, J. Mechanistic aspects of CO_2 reduction catalysis with manganese-based molecular catalysts. *Coord. Chem. Rev.* **2018**, *374*, 173−217.

(10) Yempally, V.; Moncho, S.; Hasanayn, F.; Fan, W. Y.; Brothers, E. N.; Bengali, A. A. Ancillary Ligand Effects upon the Photochemistry of Mn(bpy)$(CO)_3$X Complexes (X = Br-, $PhCC^-$). *Inorg. Chem.* **2017**, *56*, 11244−11253.

(11) Ngo, K. T.; McKinnon, M.; Mahanti, B.; Narayanan, R.; Grills, D. C.; Ertem, M. Z.; Rochford, J. Turning on the Protonation-First Pathway for Electrocatalytic CO_2 Reduction by Manganese Bipyridyl Tricarbonyl Complexes. *J. Am. Chem. Soc.* **2017**, *139*, 2604−2618.

(12) (a) Kato, E.; Takeda, H.; Koike, K.; Ohkubo, K.; Ishitani, O. Ru(II)-Re(I) binuclear photocatalysts connected by -CH_2XCH_2- (X = O, S, CH_2) for CO_2 reduction. *Chem. Sci.* **2015**, *6*, 3003−3012. (b) Rosa, A.; Ricciardi, G.; Baerends, E. J.; Stufkens, D. J. Metal-to-ligand charge transfer (MLCT) photochemistry of fac-Mn(Cl)$(CO)_3$(H-DAB): A density functional study. *J. Phys. Chem.* **1996**, *100*, 15346−15357.

(13) Koike, K.; Grills, D. C.; Tamaki, Y.; Fujita, E.; Okubo, K.; Yamazaki, Y.; Saigo, M.; Mukuta, T.; Onda, K.; Ishitani, O. Investigation of excited state, reductive quenching, and intramolecular electron transfer of Ru(II)-Re(I) supramolecular photocatalysts for CO_2 reduction using time-resolved IR measurements. *Chem. Sci.* **2018**, *9*, 2961−2974.

(14) Takeda, H.; Koizumi, H.; Okamoto, K.; Ishitani, O. Photocatalytic CO_2 reduction using a Mn complex as a catalyst. *Chem. Commun.* **2014**, *50*, 1491−1493.

https://dx.doi.org/10.1021/acs.organomet.9b00755
Organometallics XXXX, XXX, XXX−XXX